



HAL
open science

Polarized photons from the early stages of relativistic heavy-ion collisions

Sigtryggur Hauksson, Charles Gale

► **To cite this version:**

Sigtryggur Hauksson, Charles Gale. Polarized photons from the early stages of relativistic heavy-ion collisions. *Phys.Rev.C*, 2024, 109 (3), pp.034902. 10.1103/PhysRevC.109.034902 . hal-04152031

HAL Id: hal-04152031

<https://hal.science/hal-04152031>

Submitted on 11 Jul 2023

HAL is a multi-disciplinary open access archive for the deposit and dissemination of scientific research documents, whether they are published or not. The documents may come from teaching and research institutions in France or abroad, or from public or private research centers.

L'archive ouverte pluridisciplinaire **HAL**, est destinée au dépôt et à la diffusion de documents scientifiques de niveau recherche, publiés ou non, émanant des établissements d'enseignement et de recherche français ou étrangers, des laboratoires publics ou privés.



Distributed under a Creative Commons Attribution 4.0 International License

Polarized Photons from the Early Stages of Relativistic Heavy-Ion Collisions

Sigtryggur Hauksson*

Institut de Physique Théorique, CEA/Saclay, Université Paris-Saclay, 91191, Gif sur Yvette, France

Charles Gale†

Department of Physics, McGill University, 3600 University Street, Montréal, QC, Canada H3A 2T8

The polarization of real photons emitted from early-time heavy-ion collisions is calculated, concentrating on the contribution from bremsstrahlung and quark-antiquark annihilation processes at leading order in the strong coupling. The effect of an initial momentum space anisotropy of the parton distribution is evaluated using a model for the non-equilibrium scattering kernel for momentum broadening. The effect on the photon polarization is reported for different degrees of anisotropy. The real photons emitted early during in-medium interactions will be dominantly polarized along the beam axis.

I. INTRODUCTION

The theory of the nuclear strong interaction, QCD, features a transition from a phase where the relevant degrees of freedom are quarks and gluons – at high temperature – to one where the appropriate basis consists of composite hadrons at a lower temperature. This transition has been predicted by several theoretical approaches, including the non-perturbative field-theoretical framework of lattice QCD [1]. Decades of intense theoretical effort have revealed that the transition from confined hadrons to partons is not a thermodynamic phase transition in the proper sense but rather an analytic crossover [2]. On the experimental side, this exotic state of strongly interacting matter – the quark-gluon plasma (QGP) – has been observed in the relativistic collisions of nuclei (“heavy-ions”) performed at the Relativistic Heavy-Ion Collider (RHIC), and its existence has been later confirmed by experiments performed at the Large Hadron Collider (LHC) [3]. There also is strong evidence supporting the presence of QGP in smaller systems [4].

Even though new aspects of the QGP are continuously being discovered, it is fair to assert that the field is well poised to enter a phase of quantitative characterization, owing in large part to the large variety of experimental observables being measured by the experimental collaborations. Measurements designed to probe the QGP have reported results on soft hadron collective behavior [5], on QCD jet modification and energy loss [6], on photon [7] and dilepton [8] production, and on many other aspects as well. The theoretical tools developed to study the dynamics of nuclear collisions and the formation of the QGP typically consist of multistage models, rendered necessary by the complexity of the nuclear reaction. Recent examples of such a composite theoretical approach are studies [9–12] where the initial state model (e.g. $T_{\text{R}}\text{ENTo}$ [13], IP-Glasma [14]) preceded a fluid-dynamical phase ([15–18]. A hadronic cascade afterburner (e.g. UrQMD [19],

SMASH [20]), evolve the final state hadrons until their measurement. Such composite models can make statistically significant statements about transport parameters such as shear and bulk viscosity, as well as quantify the energy loss of energetic QCD jets [21].

As the multistage modeling of relativistic heavy-ion collisions covers a variety of dynamical conditions ranging from far from equilibrium initial states to almost ideal fluid dynamics, it is important to critically examine its different eras. In searching for observables capable of revealing the different modeling epochs, penetrating probes such as real and virtual photons impose themselves. Electromagnetic variables are emitted at all stages of the collision and as such can report on local conditions at their creation point [22]. The largest uncertainty in the chain of models currently lie at the beginning, in the time span preceding “hydrodynamization”. Early in the history of the collision, photon emission is liable to occur in media far from equilibrium which necessitate a dedicated theoretical treatment. The emission of photons from non-equilibrium environments has received some recent attention [23, 24].

This study will consider photon emission in the early stages of heavy-ion collisions, and will focus more specifically on the polarization states of those photons as a probe of the medium at early times. As our calculation only relies on the medium having a pressure anisotropy, or equivalently a momentum anisotropy in parton distribution, it holds both before hydrodynamization as well as in the beginning of the hydrodynamic stage while pressure anisotropy still persists. Some previous estimates for photon polarization at early times considered leading order direct photon production channels like those of the Compton process and $q\bar{q}$ annihilation [25–27]. It is known that an equally important contribution as those two – at the same order in α_s , the strong coupling constant – is that associated with the Landau-Pomeranchuk-Migdal effect (LPM) [28–30]. That contribution, evaluated for a medium out of equilibrium forms the basis of this work. It is fair to remind readers that the measurement of real photon polarization states is challenging, owing to the complications related to the external conversions into lep-

* sigtryggur.hauksson@iptt.fr

† gale@physics.mcgill.ca

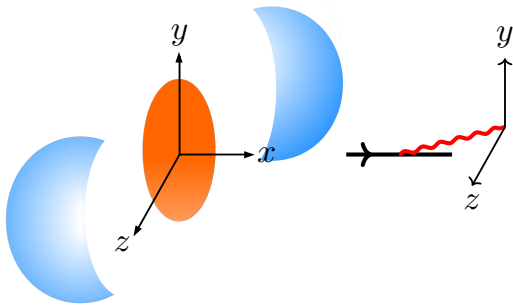


FIG. 1. Our choice of coordinate system. The z -axis is chosen to be along the beam axis. For a photon emitted at midrapidity we choose the x -axis to be along its momentum. The photon (in red) can either be transversely polarized along the beam axis (z -axis) or transversely polarized orthogonal to the beam axis, i.e. along the y -axis.

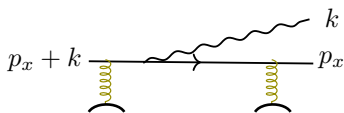


FIG. 2. Photon radiation through medium-induced bremsstrahlung off a quark

ton pairs. The angular distribution of this pairs will reflect the polarization state. A more realistic proposition is a measurement of virtual photon polarization states, as measured through an internal conversion process leading to a dilepton final state. Consequently, the goal of our work is to first set the foundations for subsequent such evaluations and to perform a first estimate of the polarization signature of an early, non-equilibrium, strongly interacting medium.

Our paper is organized as follows: Section II lays out the building blocks of our non-equilibrium formalism. The section following that one discusses the collision kernel used to model the medium interactions. The numerical methods used to obtain the production rate of polarized photons are discussed in Section IV. Results and conclusion constitute Sections V and VI, respectively. We present analytical and numerical details in the Appendices.

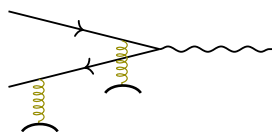


FIG. 3. Photon radiation through medium-induced quark-antiquark pair annihilation

II. POLARIZED PHOTON EMISSION

The quark-gluon plasma radiates photons through two different processes at leading order in perturbation theory. (See [31] for higher order corrections.) These processes are two-to-two scattering with a photon in the final state [32, 33], and bremsstrahlung and pair annihilation with a resulting photon [28, 30]. Two-to-two scattering on one hand and bremsstrahlung and pair annihilation on the other hand give roughly equal contribution to photon yield in the plasma [29]. While photons from two-to-two scattering have been studied extensively in an anisotropic medium and have been shown to be polarized [25], bremsstrahlung and pair annihilation photons have been studied much less in an anisotropic plasma due to the more complicated physics involved. We consider this now. Polarized photon emission has also been studied in other contexts, including in holography where a background magnetic field is included [34–36], due to vortical flow in the plasma [37], and due to the chiral magnetic effect [38, 39]. Dilepton polarization has furthermore been considered in [40–42]

In bremsstrahlung an on-shell photon is emitted collinearly off a quark or an antiquark, see Fig. 2. In vacuum this process would be kinematically forbidden as an on-shell quark cannot emit an on-shell photon. However, in a medium the process is made possible to due soft gluon kicks from the medium that bring the quark slightly off-shell. These kicks have momentum $\sim g\Lambda$ where Λ is a hard scale akin to temperature and g is the coupling constant. The off-shellness of the quark is therefore of order $P^2 \sim g^2\Lambda^2$ meaning that the emission takes time $t \sim p/P^2 \sim 1/g^2\Lambda$ where p is the quark momentum. During this time the quark can receive arbitrarily many soft gluon kicks since the mean-free time between two such kicks is also of order $1/g^2\Lambda$. All of these kicks need to be included at leading order in perturbation theory [28, 30, 43]. In an analogous fashion a quark-antiquark pair can annihilate and radiate a photon due to medium kicks, see Fig. 3.

We will now show that photons emitted through bremsstrahlung and pair annihilation are polarized in an anisotropic medium. This polarization can be described by extending the framework developed in [23, 28, 30], see App. A. To fix ideas we choose the coordinate system in Fig. 1. The z -axis lies along the beam axis in a heavy-ion collision. We consider a photon at midrapidity and orient the coordinate system so that the x -axis lies along its momentum \mathbf{k} . The momentum of the photon can of course have any direction in the plane transverse to the beam axis; aligning it with the short axis of the plasma as in Fig. 1 is simply for illustration.¹ As an on-shell photon is transversely polarized, the polarization basis can be

¹ In this work, the net polarization of photons emitted from a fluid cell is independent of the angular orientation in the transverse plane as we focus on the effect of longitudinal expansion.

chosen as $\epsilon_z = (0, 0, 0, 1)$ and $\epsilon_y = (0, 0, 1, 0)$. The photon is thus polarized along the beam axis or transverse to the beam axis.

In Appendix A we show that the rate of producing z -polarized photons with momentum k through bremsstrahlung is

$$k \frac{d\Gamma_z}{d^3\mathbf{k}} = \frac{6\alpha_{EM} \sum_s q_s^2}{(2\pi)^3} 2 \int_0^\infty dp_x \frac{k}{8p_x^2(k+p_x)} \times n_f(k+p_x) [1 - n_f(p_x)] (F_{\text{in}}(\zeta)A_z + F_{\text{out}}(\zeta)A_y) \quad (1)$$

where momenta are defined in Fig. 2 and $\zeta = k/(p_x + k)$ is the momentum fraction of the photon. Similarly, the rate of producing y -polarized photons is

$$k \frac{d\Gamma_y}{d^3\mathbf{k}} = \frac{6\alpha_{EM} \sum_s q_s^2}{(2\pi)^3} 2 \int_0^\infty dp_x \frac{k}{8p_x^2(k+p_x)} \times n_f(k+p_x) [1 - n_f(p_x)] (F_{\text{in}}(\zeta)A_y + F_{\text{out}}(\zeta)A_z) \quad (2)$$

where A_z and A_y have been interchanged relative to Eq. (1). Here A_z and A_y quantify the amount of momentum broadening in the z - and y -direction and are defined as

$$\begin{aligned} A_z &= \text{Re} \int \frac{d^2\mathbf{p}_\perp}{(2\pi)^2} 2p_z f_z(\mathbf{p}_\perp) \\ A_y &= \text{Re} \int \frac{d^2\mathbf{p}_\perp}{(2\pi)^2} 2p_y f_y(\mathbf{p}_\perp) \end{aligned} \quad (3)$$

where \mathbf{f} solves an integro-differential equation given below. Furthermore,

$$F_{\text{in}}(\zeta) = \frac{(2-\zeta)^2}{\zeta} \quad (4)$$

and

$$F_{\text{out}}(\zeta) = \zeta, \quad (5)$$

are polarized splitting functions [44]. Finally, there are momentum factors n_f for the incoming and outgoing quarks.² The analogous expressions for quark-antiquark pair annihilation are given in Appendix A.

Eqs. (1) and (2) for polarized photon emission can be understood intuitively. We consider a z -polarized photon for concreteness. As the photon travels in the x -direction, the splitting plane of the photon and the outgoing quark is spanned by $\hat{\mathbf{e}}_x$ and a vector orthogonal to $\hat{\mathbf{e}}_x$ which we call $\hat{\mathbf{n}}$, see Fig. 4. Eqs. (1) and (2) show that we can project the vector $\hat{\mathbf{n}}$ on to the y - and the z -axes and sum over the contributions. For $\hat{\mathbf{n}}$ in the z -direction, the

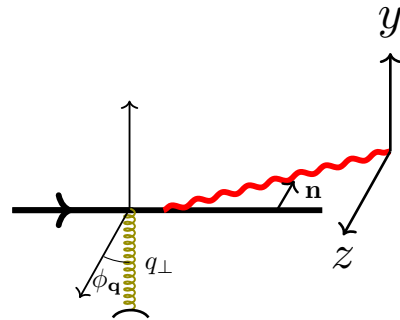


FIG. 4. Definition of the quantities $\hat{\mathbf{n}}$ (the vector between the outgoing quark and photon) and $\phi_{\mathbf{q}}$ (the angle defining a soft gluon kick of magnitude q_\perp). The photon can be polarized in the y - or the z -directions which are transverse to its direction of motion, see also Fig. 1.

z -polarized photon is polarized in the splitting plane and the hard splitting function is F_{in} . Momentum broadening is quantified by the z -component A_z . On the other hand, for $\hat{\mathbf{n}}$ in the y -direction, the z -polarized photon is polarized out of the splitting plane and the hard splitting function is F_{out} . Momentum broadening is then quantified by A_y .

The rate equations for photon emission depend on the function $\mathbf{f} = (f_z, f_y)$ which quantifies momentum broadening. It solves the integro-differential equation

$$2\mathbf{p}_\perp = i\delta E \mathbf{f}(\mathbf{p}_\perp) + \int \frac{d^2q_\perp}{(2\pi)^2} \mathcal{C}(\mathbf{q}_\perp) [\mathbf{f}(\mathbf{p}_\perp) - \mathbf{f}(\mathbf{p}_\perp + \mathbf{q}_\perp)] \quad (6)$$

where

$$\delta E = \frac{k}{2p(p+k)} [p_\perp^2 + m_\infty^2]. \quad (7)$$

The central ingredient in this equation is the collision kernel $\mathcal{C}(\mathbf{q}_\perp)$ which gives the rate for a quark to receive soft gluon kicks of transverse momentum \mathbf{q}_\perp . The collision kernel gives rise to a gain term and a loss term in Eq. (6).

In an isotropic medium, the collision kernel is by definition isotropic, $\mathcal{C}(\mathbf{q}_\perp) = \mathcal{C}(q_\perp)$ and one can show that $\mathbf{f} = \mathbf{p}_\perp \hat{f}(p_\perp)$. This means that $A_z = A_y$ and thus there is no net polarization of photons emitted. In an anisotropic medium, $\mathcal{C}(\mathbf{q}_\perp)$ depends not only on the magnitude of the kick q_\perp but also on its orientation. In other words, when writing

$$\mathbf{q}_\perp = (q_z, q_y) = q_\perp (\cos \phi_{\mathbf{q}}, \sin \phi_{\mathbf{q}}) \quad (8)$$

the collision kernel depends on both $\phi_{\mathbf{q}}$ and q_\perp , see Fig. 4. This leads to \mathbf{f} having more complicated angular dependence so that $A_z \neq A_y$. Therefore, photon emission from an anisotropic medium is polarized.

This could be generalized to include transverse expansion which breaks this symmetry. Our formalism could also easily be extended to photons at finite rapidity.

² We have assumed that there is no chiral imbalance in the medium and that the baryon chemical potential vanishes, so that quarks and antiquarks of both helicities have the same momentum distribution n_f .

III. MODEL OF THE COLLISION KERNEL IN AN ANISOTROPIC PLASMA

As previously argued, the collision kernel for soft gluon kicks $\mathcal{C}(\mathbf{q}_\perp)$ is anisotropic in heavy-ion collisions which leads to polarization of photons emitted through bremsstrahlung. The ultimate source of the anisotropy in the kernel is longitudinal expansion of the medium along the beam axis. Such a longitudinal expansion gives pressure anisotropy at early and intermediate times with longitudinal pressure P_L less than transverse pressure P_T . On a microscopic level, this means that quark and gluon quasiparticles have an anisotropic momentum distribution with $\langle p_z^2 \rangle < \langle p_x^2 \rangle, \langle p_y^2 \rangle$. This is captured by the distribution introduced in Ref. [45]:

$$f(\mathbf{p}) = \sqrt{1 + \xi} f_{\text{iso}}(\sqrt{\mathbf{p}^2 + \xi p_z^2}) \quad (9)$$

where f_{iso} is an isotropic distribution, and $\xi > 0$ quantifies the degree of anisotropy. The prefactor $\sqrt{1 + \xi}$ ensures that the number density of quarks and gluons is the same as in equilibrium. A simple calculation gives the pressure anisotropy P_T/P_L in terms of the momentum space anisotropy ξ , linking the macroscopic and microscopic descriptions.³

Ideally, one would want to calculate the collision kernel for momentum broadening, $\mathcal{C}(\mathbf{q}_\perp)$, directly from Eq. (9). Such a calculation would use that the hard quasiparticles in Eq. (9) radiate soft gluons which are then responsible for momentum broadening. This would allow to quantify the degree of photon polarization in a non-equilibrium medium from first principles. Unfortunately, going from Eq. (9) to the collision kernel is difficult in practice, partially due to instabilities that can be present in an anisotropic plasma [47].

In this study, we will use a simple model of the collision kernel in a longitudinally expanding medium. We take inspiration from results for the collision kernel in thermal equilibrium at leading order in perturbation theory [48],

$$\mathcal{C}_{\text{eq}}(\mathbf{q}_\perp) = g^2 C_F T \left(\frac{1}{q_\perp^2} - \frac{1}{q_\perp^2 + m_{D0}^2} \right) \quad (10)$$

Here m_{D0}^2 is the equilibrium Debye mass which describes screening of electric fields. (The equilibrium kernel has furthermore been evaluated at next-to-leading order [49], as well as on the lattice, see e.g. [50, 51].) In our anisotropic model, we replace the equilibrium Debye mass by its anisotropic extension⁴ found in [45]

$$m_D^2(\phi_{\mathbf{q}}) = \left(1 - \frac{2\xi}{3} \right) m_{D0}^2 + \xi m_{D0}^2 \cos^2 \phi_{\mathbf{q}}. \quad (11)$$

so that

$$\mathcal{C}(\mathbf{q}_\perp) = g^2 C_F \Lambda \left(\frac{1}{q_\perp^2} - \frac{1}{q_\perp^2 + m_D^2(\phi_{\mathbf{q}})} \right) \quad (12)$$

The anisotropic correction has an angular dependence with more broadening in the z -direction than in the y -direction. To simplify calculations, we expand the collision kernel in ξ , writing

$$\mathcal{C}(\mathbf{q}_\perp) \approx g^2 C_F \Lambda \left(\frac{1}{q_\perp^2} - \frac{1}{q_\perp^2 + m_{D0}^2} + \frac{-2\xi m_{D0}^2/3 + \xi m_{D0}^2 \cos^2 \phi_{\mathbf{q}}}{(q_\perp^2 + m_{D0}^2)^2} \right) \quad (13)$$

where Λ is a hard scale, akin to temperature.

Eq. (13) is a toy model for the collision kernel, intended to illustrate how an anisotropic kernel leads to polarized photon emission and to estimate the magnitude of this effect. This toy model only includes changes to the screening of electric fields in an anisotropic medium and not the myriad other non-equilibrium effects that can arise. Nevertheless, this collision kernel can be motivated by theoretical arguments making us believe that it captures some of the salient features of the full non-equilibrium kernel.

In general the collision kernel is defined by

$$\mathcal{C}(\mathbf{q}_\perp) = g^2 C_F \int \frac{dq^0 dq_x}{(2\pi)^2} D_{rr}^{\mu\nu}(Q) v_\mu v_\nu 2\pi \delta(v \cdot Q) \quad (14)$$

where $v^\mu = (1, 1, 0, 0)$ is the four-velocity of the quark emitting a photon. The kernel depends on the statistical correlator for gluons in the medium,

$$D_{rr}(Q) := \frac{1}{2} \langle \{A, A\} \rangle(Q) = D_{\text{ret}}(Q) \Pi(Q) D_{\text{adv}}(Q) \quad (15)$$

which characterizes the occupation density of a pair of soft gluons. We have omitted Lorentz indices for simplicity. This statistical correlator contains information on how the soft gluons are emitted by hard quasiparticles with rate $\Pi(Q)$ and then propagate in the medium according to the retarded propagator $D_{\text{ret}}(Q) = i/(Q^2 - \Pi_{\text{ret}})$ and the advanced propagator $D_{\text{adv}} = -D_{\text{ret}}^*$.

Making some heuristic assumptions allows one to employ a sum rule in [48] to motivate the toy model for the collision kernel in Eq. (13), starting from the definitions in Eqs. (14) and (15). The goal is to include anisotropic corrections to the screening of chromoelectric fields, while ignoring anisotropic corrections to the density of gluons and to change in polarization that occurs during propagation. We work strictly at small anisotropy $\xi \ll 1$, including only effects of order $\mathcal{O}(\xi)$.

The first heuristic assumption is to employ the identity $\Pi(Q) = \frac{\Lambda}{q^0} 2\text{Im} \Pi_{\text{ret}}$ which is known as the KMS identity and which expresses detailed balance between production and decay of soft gluons. This is not strictly valid in a non-equilibrium medium and amounts to ignoring

³ Specifically, $P_T/P_L = \frac{1}{2} \frac{\sqrt{\xi} + (\xi-1) \arctan \sqrt{\xi}}{\arctan \sqrt{\xi} - \sqrt{\xi}/(1+\xi)}$, see e.g. [46].

⁴ In [45] this quantity is referred to as m_\perp^2 . We have expanded in small ξ in Eq. (13) but this is simply for convenience and not fundamental to the setup we use.

anisotropic corrections to the density of gluons. Then one can write

$$D_{rr}(Q) := \frac{\Lambda}{q^0} (D_{\text{ret}} - D_{\text{adv}}). \quad (16)$$

At small anisotropy the retarded propagator in Eq. (16) is

$$D_{\text{ret}}^{\mu\nu}(Q) \approx \frac{P_T^{\mu\nu}}{Q^2 - \Pi_T} + \frac{P_L^{\mu\nu}}{Q^2 - \Pi_L}. \quad (17)$$

Here we have only included anisotropic corrections to the screening as given by Π_T and Π_L , see App. B.

Our second heuristic approximation is to focus on the anisotropic correction to Π_L and ignore those in Π_T . Comparing with the equilibrium calculation [48], this amounts to calculating anisotropic corrections to the term $1/(q_\perp^2 + m_{D0}^2)$ in Eq. (10) while leaving the term $1/q_\perp^2$ as is. This means that we include anisotropic corrections to the screening of chromoelectric fields as given by a Debye mass but do not include anisotropic corrections to the screening of chromomagnetic fields.

The reason we use this approximation is that the sum rule we employ does not work for the transverse screening in Π_T . This is because the term $1/(Q^2 - \Pi_T)$ has a pole in the upper half complex plane of q_0 corresponding to Weibel instabilities [52]. A formal use of the sum rule would lead to a contribution of the form $1/(q_\perp^2 - m^2)$ which is ill-defined at $q_\perp = m$. The solution to this issue is to use a retarded propagator for soft gluons that includes the mechanism by which non-Abelian interaction caps the growth of the unstable soft gluon modes. This is beyond the scope of this project.

Given these two approximations, one can use the sum rule in [48] nearly directly. The longitudinal retarded self-energy at small anisotropy ξ is

$$\begin{aligned} \Pi_L(Q) = \Pi_L^0(x) + \xi \left[\frac{1}{6} (1 + 3 \cos 2\theta_n) \frac{Q^2}{q^2} m_{D0}^2 \right. \\ \left. + \Pi_L^0(x) \left(\cos 2\theta_n - \frac{x^2}{2} (1 + 3 \cos 2\theta_n) \right) \right] \end{aligned} \quad (18)$$

where θ_n is the angle between \mathbf{q} and the anisotropy vector $\mathbf{n} = \mathbf{e}_z$ which defines a preferred direction in Eq. (9) [45]. Here

$$\Pi_L^0(x) = (x^2 - 1) m_{D0}^2 \left[\frac{x}{2} \log \frac{x + 1 + i\epsilon}{x - 1 + i\epsilon} - 1 \right] \quad (19)$$

is the equilibrium value. We next do a change of variables in Eq. (14) to $x = q_0/q = q_x/\sqrt{q_x^2 + q_\perp^2}$ so that $q_x^2 = x^2 q_\perp^2/(1 - x^2)$ and $q^2 = q_\perp^2/(1 - x^2)$. Then one should substitute $\cos 2\theta_n = 2(q_z/q)^2 - 1 = 2(1 - x^2) \cos^2 \phi_{\mathbf{q}} - 1$ to get dependence only on x , q_\perp and $\phi_{\mathbf{q}}$. This gives that the longitudinal contribution to the collision kernel is

$$\frac{\Lambda g^2 C_F}{\pi} \int_0^1 \frac{dx}{x} \frac{\text{Im} \tilde{\Pi}_L(x, \phi_{\mathbf{q}})}{\left(q_\perp^2 + \text{Re} \tilde{\Pi}_L(x, \phi_{\mathbf{q}}) \right)^2 + \left(\text{Im} \tilde{\Pi}_L(x, \phi_{\mathbf{q}}) \right)^2}. \quad (20)$$

where

$$\begin{aligned} \tilde{\Pi}_L(x, \phi_{\mathbf{q}}) = \Pi_L^0(x) + \xi \left[\frac{1}{6} (1 + 3 \cos 2\theta_n) (x^2 - 1) m_{D0}^2 \right. \\ \left. + \Pi_L^0(x) \left(\cos 2\theta_n - \frac{x^2}{2} (1 + 3 \cos 2\theta_n) \right) \right] \Big|_{\cos 2\theta_n = 2(1-x^2) \cos^2 \phi_{\mathbf{q}} - 1} \end{aligned} \quad (21)$$

has no explicit dependence on q_\perp .

@articleAurenche:2002pd, @articleAurenche:2002pd, An argument nearly identical⁵ to the one in [48] then shows that Eq. (20) is

$$\begin{aligned} g^2 C_F \Lambda \left[\frac{1}{q_\perp^2 + \lim_{x \rightarrow \infty} \tilde{\Pi}_L(x, \phi)} - \frac{1}{q_\perp^2 + \tilde{\Pi}_L(0, \phi)} \right] \\ = -g^2 C_F \Lambda \frac{1}{q_\perp^2 + m_D^2(\phi_{\mathbf{q}})} \end{aligned} \quad (22)$$

since $\tilde{\Pi}_L(0, \phi) = m_D^2(\phi_{\mathbf{q}})$. Our conclusion is therefore that given our heuristic approximations, the collision kernel is given by Eq. (13). We emphasize that this collision kernel is not intended to capture all of the non-equilibrium physics but to focus on anisotropic corrections to the screening of chromoelectric fields.

IV. NUMERICAL METHOD

We wish to evaluate the rate of polarized photon emission in an anisotropic medium such as that found in a longitudinally expanding quark-gluon plasma. The starting point is Eqs. (1) and (2) which require solving the integro-differential equation in Eq. (6) numerically, assuming the model for the collision kernel given in Eq. (13). To solve Eq. (6) we go to impact parameter space, i.e. the space Fourier conjugate to \mathbf{p}_\perp . Defining

$$\mathbf{f}(\mathbf{b}) = \int \frac{d^2 p_\perp}{(2\pi)^2} e^{i\mathbf{p}_\perp \cdot \mathbf{b}} \mathbf{f}(\mathbf{p}_\perp). \quad (23)$$

the equation we wish to solve becomes

$$-2i\nabla_b \delta^{(2)}(\mathbf{b}) = \frac{ik}{2p(p+k)} \left[-\nabla_b^2 + m_\infty^2 \right] \mathbf{f}(\mathbf{b}) + \mathcal{C}(\mathbf{b}) \mathbf{f}(\mathbf{b}). \quad (24)$$

⁵ The retarded propagator $1/[x^2 q_\perp^2 - q_\perp^2 - (1-x^2)\Pi_L(x, \phi)]$ in Eq. 7 in [48] has an extra pole in the upper half complex plane in the anisotropic case. This pole can be seen by taking the limit $x = k_0/k \rightarrow \infty$ in which case the propagator becomes $\sim 1/(1-x^2)/(q_\perp^2 + (\frac{1}{3} - \frac{1}{3}\xi \cos^2 \phi) m_{D0}^2 + \frac{\xi}{3} x^2 \cos^2 \phi m_{D0}^2)$ which has a pole which is parametrically of the form $x \sim \pm i q_\perp / m_D \sqrt{\xi}$ and thus far from the real axis when $\xi \ll 1$. This is not in contradiction with the usual properties of the retarded propagator as we have imposed $q_0 = q_x$ and then search for poles in q_0 . One can then show that the correction due to this pole to the sum rule in Eq. 9 in [48] is $\mathcal{O}(\xi^{3/2})$ which is subleading to the $\mathcal{O}(\xi)$ contributions we consider.

where

$$\mathcal{C}(\mathbf{b}) = \int \frac{d^2 p_\perp}{(2\pi)^2} [1 - e^{i\mathbf{p}_\perp \cdot \mathbf{b}}] \mathcal{C}(\mathbf{p}_\perp). \quad (25)$$

A straightforward calculation shows that the collision kernel from Eq. (13) is

$$\mathcal{C}(\mathbf{b}) = \mathcal{C}_0(b) + \xi \mathcal{C}_1^{(a)}(b) + \xi \cos 2\beta \mathcal{C}_1^{(b)}(b) \quad (26)$$

in impact parameter space where $\mathbf{b} = (b_z, b_y) = (\cos \beta, \sin \beta) b$. The terms of the collision kernel are given by

$$\mathcal{C}_0(\mathbf{b}) = \frac{g^2 C_{FT}}{2\pi} \left[K_0(m_{D0}b) + \gamma_E + \log \frac{m_{D0}b}{2} \right], \quad (27)$$

$$\mathcal{C}_1^{(a)}(b) = g^2 C_{FT} \frac{1}{8\pi} \frac{M^2}{m_{D0}^2} (m_{D0}b K_1(m_{D0}b) - 1) \quad (28)$$

and

$$\mathcal{C}_1^{(b)}(b) = g^2 C_{FT} \frac{M^2 b^2}{4\pi} \left[\frac{2}{(m_{D0}b)^4} - \frac{1}{2m_{D0}b} K_1(m_{D0}b) - \frac{1}{(m_{D0}b)^2} K_2(m_{D0}b) \right] \quad (29)$$

In order to solve Eq. (24) we do an expansion in small ξ , giving

$$\mathbf{f}(\mathbf{b}) = \mathbf{f}_0(\mathbf{b}) + \xi \mathbf{f}_1(\mathbf{b}) + \dots \quad (30)$$

The zeroth order solution in ξ satisfies the usual isotropic equation

$$\frac{ik}{2p(p+k)} [-\nabla_b^2 + m_\infty^2] \mathbf{f}_0(\mathbf{b}) + \mathcal{C}_0(b) \mathbf{f}_0(\mathbf{b}) = -2i \nabla_b \delta^{(2)}(\mathbf{b}) \quad (31)$$

and can be shown to have angular dependence $\mathbf{f}_0(\mathbf{b}) \sim (\cos \beta, \sin \beta)$. The first order satisfies

$$\begin{aligned} \frac{ik}{2p(p+k)} [-\nabla_b^2 + m_\infty^2] \mathbf{f}_1(\mathbf{b}) + \mathcal{C}_0(b) \mathbf{f}_1(\mathbf{b}) \\ = - \left[\mathcal{C}_1^{(a)}(b) + \cos 2\beta \mathcal{C}_1^{(b)}(b) \right] \mathbf{f}_0(\mathbf{b}). \end{aligned} \quad (32)$$

Due to the angular dependence of the right hand side we can write in full generality

$$f_{1z}(\mathbf{b}) = \cos \beta f_1^{(1z)}(b) + \cos 3\beta f_1^{(3)}(b) \quad (33)$$

and

$$f_{1y}(\mathbf{b}) = \sin \beta f_1^{(1y)}(b) + \sin 3\beta f_1^{(3)}(b) \quad (34)$$

where these functions solve

$$\mathcal{K} [f_1^{(1z)}(\mathbf{b})] + \mathcal{C}_0(b) f_1^{(1z)}(\mathbf{b}) = - \left[\mathcal{C}_1^{(a)}(b) + \frac{1}{2} \mathcal{C}_1^{(b)}(b) \right] f_0, \quad (35)$$

$$\mathcal{K} [f_1^{(1y)}(\mathbf{b})] + \mathcal{C}_0(b) f_1^{(1y)}(\mathbf{b}) = - \left[\mathcal{C}_1^{(a)}(b) - \frac{1}{2} \mathcal{C}_1^{(b)}(b) \right] f_0 \quad (36)$$

with

$$\mathcal{K} [\mathbf{f}(\mathbf{b})] = - \frac{ik}{2p(p+k)} \left[\frac{d^2}{db^2} + \frac{1}{b} \frac{d}{db} - \frac{1}{b^2} - m_\infty^2 \right] \mathbf{f}(\mathbf{b}). \quad (37)$$

(The differential equation for $f_1^{(3)}$ is given in App. C.)

Our goal is to evaluate

$$A_z = 2\text{Im} \partial_{b_z} f_z(\mathbf{b}) \Big|_{b=0} = 2\text{Im} \frac{\hat{\mathbf{b}} \cdot \mathbf{f}_0 + \xi f_1^{(1z)}}{b} \Big|_{b=0} \quad (38)$$

and

$$A_y = 2\text{Im} \partial_{b_y} f_y(\mathbf{b}) \Big|_{b=0} = 2\text{Im} \frac{\hat{\mathbf{b}} \cdot \mathbf{f}_0 + \xi f_1^{(1y)}}{b} \Big|_{b=0} \quad (39)$$

which were defined in Eqs. (1) and (2). Thus, we only need to know $f_1^{(1z)}(b)/b$ and $f_1^{(1y)}(b)/b$ in the limit $b \rightarrow 0$ where it must be finite. This gives the boundary condition that This is done by demanding that $f_1^{(1z)}$ and $f_1^{(1y)}$ vanish at $b = 0$. The other boundary condition is that the functions vanish as $b \rightarrow \infty$ as can be seen from Eq. (23).

To evaluate $f_1^{(1z)}(b)/b$ and $f_1^{(1y)}(b)/b$ at $b = 0$, we demand that the functions $f_1^{(1z)}$ and $f_1^{(1y)}$ vanish at very large b and evolve the functions numerically to small b using Eqs. (35) and (36). In practice, this means that we start the evolution at a large but finite value of b where $f_1^{(1z)}$ and $f_1^{(1y)}$ are initialized to a small value. A typical numerical solution for f_1^{1z} and f_1^{1y} then blows up as evolved towards $b \rightarrow 0$. We must then extract the finite part of our numerical solution. This is done by matching with known, analytic solutions of the differential equations in the small b limit.

For instance, focusing on Eq. (35), we call the particular solution $w(b)$ and the two independent solutions of the homogeneous equation $w_1(b)$ and $w_2(b)$. These are known analytically at small b , see Appendix C. We can write our numerical solution in full generality at small b as

$$f_1^{(1z)}(b) = w(b) + \alpha_1 w_1(b) + \alpha_2 w_2(b) \quad (40)$$

where α_1 and α_2 are found numerically. To extract from this a solution with the right behaviour as $b \rightarrow 0$, one must in essence subtract a linear combination of w_1 and w_2 which satisfies the boundary condition at $b \rightarrow \infty$. Then one is left with a solution which satisfies boundary conditions both at $b = 0$ and $b \rightarrow \infty$ and which gives $f_1^{(1z)}(b)/b$ at $b = 0$. This procedure is explained in further detail in Appendix C, see also [48, 53, 54] for earlier work in the isotropic case. A major difference with the isotropic case is that Eqs. (35) and (36) have a non-trivial right hand side which complicates the matching

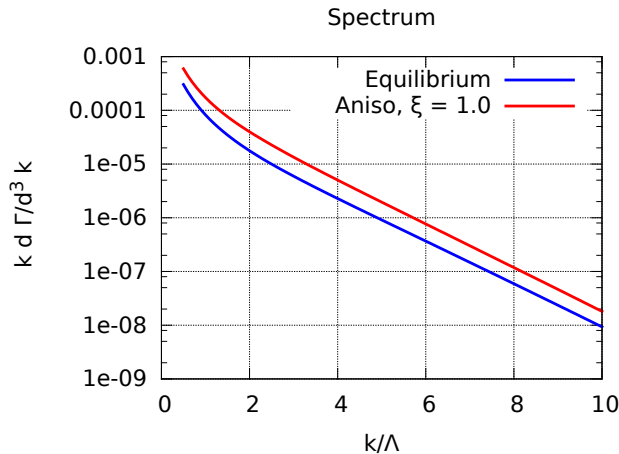


FIG. 5. Spectrum of photons coming from bremsstrahlung and pair annihilation in a plasma at effective temperature Λ . The anisotropic plasma has $\xi = 1.0$.

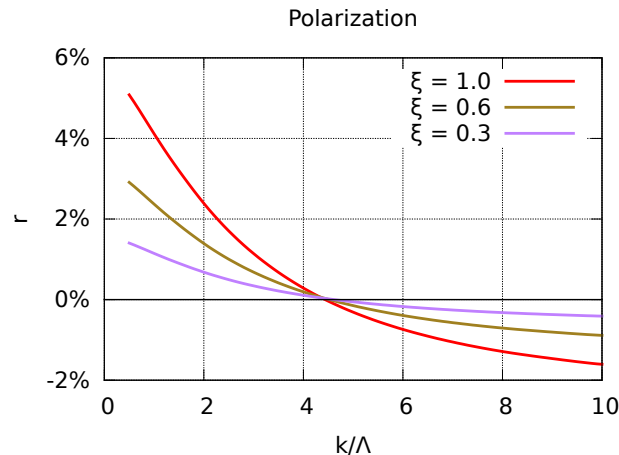


FIG. 6. Degree of polarization of photons emitted from bremsstrahlung and pair annihilation in an anisotropic plasma with $\xi = 1.0$. The quantity R is defined in Eq. (43).

procedure. For instance, one must find an analytic solution $w(b)$ of the full differential equations at small b , including the right hand side. Furthermore, cancellation errors between solutions of the full differential equation and the homogeneous equation must carefully be avoided to get reliable results, see Appendix C.

V. RESULTS

Figs. 5 and 6 are the main results of this work. They show the rate of photon production through bremsstrahlung and pair-annihilation in an anisotropic quark-gluon plasma with fixed anisotropy ξ . The collision kernel is given by Eq. (13) while the momentum

distribution of medium quarks is

$$f(\mathbf{p}) = \frac{\sqrt{1+\xi}}{e\sqrt{p^2+\xi p_z^2/\Lambda} + 1} \quad (41)$$

where Λ can be seen as an effective temperature. Fig. 5 shows the total rate for producing photons at mid-rapidity and with momentum k , i.e.

$$k \frac{d\Gamma}{d^3\mathbf{k}} = k \frac{d\Gamma_z}{d^3\mathbf{k}} + k \frac{d\Gamma_y}{d^3\mathbf{k}}, \quad (42)$$

where $k \frac{d\Gamma_z}{d^3\mathbf{k}}$ is the rate of producing photons polarized along the beam axis and $k \frac{d\Gamma_y}{d^3\mathbf{k}}$ is the rate for photons polarized orthogonal to the beam axis and to the photon momentum. Fig. 6 shows the degree of polarization at different momenta defined as

$$R = \frac{k \frac{d\Gamma_z}{d^3\mathbf{k}} - k \frac{d\Gamma_y}{d^3\mathbf{k}}}{k \frac{d\Gamma_z}{d^3\mathbf{k}} + k \frac{d\Gamma_y}{d^3\mathbf{k}}}. \quad (43)$$

These quantities are shown for three values of anisotropy parameter, $\xi = 0.3$, $\xi = 0.6$ and $\xi = 0.9$, which correspond to pressure anisotropy of $P_L/P_T \approx 0.81$, $P_L/P_T \approx 0.68$ and $P_L/P_T \approx 0.57$ respectively. These are rather moderate values of pressure anisotropy which can be found in the early and intermediate stages of heavy-ion collisions.

The spectrum in an anisotropic medium is higher than that in an equilibrium medium at the same effective temperature Λ , as can be seen in Fig. 5. This is due to the factor $\sqrt{1+\xi}$ in the momentum distribution in Eq. (9) which increases the number of quarks with $p_z = 0$ which can emit photons at midrapidity. This effect is partially compensated by anisotropic corrections which reduce the collision kernel $\mathcal{C}(\mathbf{q}_\perp)$ meaning that a given quark receives less momentum broadening, reducing the rate at which it emits photons collinearly.

More interesting is the polarization R as a function of momentum k . As seen in Fig. 6, the polarization has different signs for lower and higher values of the photon energy k : it is along the beam axis for lower values of k while it is orthogonal to the beam axis at higher values of k . This owes to the interplay between bremsstrahlung and pair annihilation. As shown in Appendix A, because of the different polarized splitting functions, bremsstrahlung tends to give photons polarized along the z -axis, while pair annihilation tends to give polarization along the x -axis, see Fig. 1. As bremsstrahlung is suppressed at high k (there are few medium quarks with energy higher than k) x -polarization dominates in that regime. On the contrary, pair annihilation is suppressed at low k since the number of quarks with energy less than $k/2$ is phase space suppressed. This gives z -polarized photons in that regime.

Despite the complicated dependence of polarization on photon momentum, polarization along the beam axis dominates. This is simply because there are many more

photons at lower k and thus their polarization is dominant. Furthermore, in [25] it was shown that photons from two-to-two scattering, which are equally important as bremsstrahlung and pair annihilation photons, are also predominantly polarized along the beam axis, with an even greater magnitude of polarization. Thus a definite prediction of our work is that medium photons are polarized along the beam axis.

To make contact with potential experiments on photon polarization more work is needed. Firstly, all photon sources that cannot be subtracted in experiments need to be included, such as prompt photons and photons from the hadronic stage. Secondly, calculation of the rate of photon production in an anisotropic medium need to be folded with hydrodynamic or kinetic theory simulations of the medium to get a realistic evolution of the medium anisotropy.

VI. CONCLUSION

In this work, we have calculated for the first time the degree of polarization for photons emitted in bremsstrahlung and off-shell pair annihilation processes in a hot medium consisting of quarks and gluons. Our evaluation includes the LPM regime and is at complete leading order in the strong coupling. The polarization of the real photons originating from bremsstrahlung and annihilation processes depends on the anisotropy of the original parton distribution, and therefore the polarization can instruct us on the dynamics in an environment that is not accessible to the vast majority of probes and observables measured in relativistic heavy-ion collisions. Specifically, it gives a measure of the pressure anisotropy at early times.

We trust that the methods and techniques developed and used here will be useful in the evaluations of polarization signatures of real and virtual photons, evaluated with scattering kernels for momentum broadening derived from microscopic theories and using time-evolution models based in QCD.

ACKNOWLEDGMENTS

C. G. acknowledges the support of the Natural Sciences and Engineering Research Council of Canada (NSERC), SAPIN-2020-00048.

Appendix A: Derivation of rate equations

We wish to show that the total rate for polarized photon production through bremsstrahlung and pair annihilation

can be written as

$$k \frac{d\Gamma_z}{d^3\mathbf{k}} = \frac{6\alpha_{EM} \sum_s q_s^2}{(2\pi)^3} \int_{-\infty}^{\infty} dp^z F(\mathbf{k} + \mathbf{p}) [1 - F(\mathbf{p})] \times \frac{1}{2} \frac{1}{4(p^x)^2(p^x + k)^2} [(2p^x + k)^2 A_z + k^2 A_y] \quad (\text{A1})$$

and

$$k \frac{d\Gamma_y}{d^3\mathbf{k}} = \frac{6\alpha_{EM} \sum_s q_s^2}{(2\pi)^3} \int_{-\infty}^{\infty} dp^z F(\mathbf{k} + \mathbf{p}) [1 - F(\mathbf{p})] \times \frac{1}{2} \frac{1}{4(p^x)^2(p^x + k)^2} [k^2 A_z + (2p^x + k)^2 A_y] \quad (\text{A2})$$

where A_z and A_y are defined in Eq. (3). Here the momentum distributions are contained in

$$F(p^x) = \theta(p^x) f(\mathbf{p}) + \theta(-p^x) (1 - f(-\mathbf{p})). \quad (\text{A3})$$

Looking at the momentum factors in Eqs. (A1) and (A2), we see that bremsstrahlung off a quark or an antiquark corresponds to $p^x > 0$ and $p^x < -k$. These cases can be rewritten to give Eqs. (1) and (2). Furthermore, $-k < p^x < 0$ corresponds to quark-antiquark pair annihilation. As the quark moves in the same direction as the photon we can set e.g. $f(\mathbf{p}) = f(p^x)$.

The derivation of polarized photon emission in Eqs. (A1) and (A2) is similar to that for unpolarized emission found in [23, 28, 30]. The polarized rate comes from evaluating the diagram in Fig. 8. The gluon ladders which represent soft kicks from the medium are evaluated in the same way as for unpolarized photon emission. Physically, this is because the soft kicks do not have enough energy to flip the helicity of quarks. The gluon ladders are summed to all orders to give the integral equation in Eq. (6). On the contrary, one must keep track of polarization at the hard emission vertices to evaluate the polarized emission rate.

For a bare quark loop without soft gluon kicks, Fig. 7, the hard emission vertices for a z -polarized photon take the form

$$H^{zz} := \epsilon_\mu^z \epsilon_\nu^{z*} \text{Tr} [\gamma^\mu (\not{K} + \not{P}) \gamma^\nu \not{P}]. \quad (\text{A4})$$

Here ϵ_μ^z is the photon polarization tensor for z -polarization. This trace is most easily evaluated by using that e.g.

$$\not{P} = \sum_s u^s(\mathbf{p}) \bar{u}^s(\mathbf{p}) \quad (\text{A5})$$

where the sum is over spin states and

$$u^s(\mathbf{p}) = \sqrt{2p} \begin{bmatrix} \frac{1-\sigma \cdot \hat{\mathbf{p}}}{2} \xi^s \\ \frac{1+\sigma \cdot \hat{\mathbf{p}}}{2} \xi^s \end{bmatrix} \quad (\text{A6})$$

are helicity states of quarks [55]. Here ξ^s form a basis for two-component spin states. One can then show by an explicit calculation that

$$H^{zz} = \sum_{s,t} [\gamma^z u^s(\mathbf{p} + \mathbf{k}) \bar{u}^s(\mathbf{p} + \mathbf{k}) \gamma^z u^t(\mathbf{p}) \bar{u}^t(\mathbf{p})] = \frac{8p(p+k)}{p^2(p+k)^2} [(2p+k)^2 p_{\perp z}^2 + k^2 p_{\perp y}^2]. \quad (\text{A7})$$

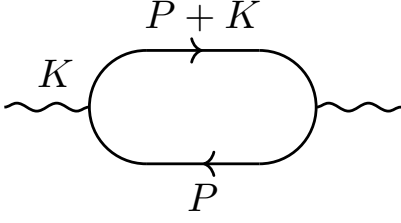


FIG. 7. Definition of momenta in photon emission.

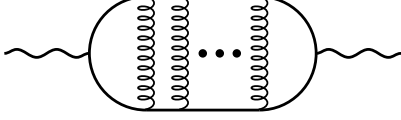


FIG. 8. Diagram for medium-induced photon emission. The gluon rungs are responsible for momentum broadening.

Similarly, the hard emission vertices for emission of y -polarized photons are

$$H^{yy} = \frac{8p(p+k)}{p^2(p+k)^2} [(2p+k)^2 p_{\perp y}^2 + k^2 p_{\perp z}^2]. \quad (\text{A8})$$

This is the same as Eq. (A7), except that $p_{\perp z}^2$ and $p_{\perp y}^2$ have been interchanged.

To include soft gluon as in Fig. 8 one simply replaces one of the hard vertices by the dressed vertex $\mathbf{f}(\mathbf{p}_{\perp})$ which includes gluons rungs and obeys the integral equation in Eq. (6). This means that in Eqs. (A7) and (A8) one replaces $p_{\perp z}^2 \rightarrow p_{\perp z} f_z$ and $p_{\perp y}^2 \rightarrow p_{\perp y} f_y$. This reproduces Eqs. (A1) and (A2).

Appendix B: The retarded gluon propagator at small anisotropy

In a system whose hard quasiparticles have the momentum distribution in Eq. (9), the retarded propagator for soft gluons is [45, 47]

$$D_{\text{ret}}^{\mu\nu}(Q) = (P_T^{\mu\nu} - C^{\mu\nu}) D_{\text{ret}}^B + [(Q^2 - \Pi_c) P_L^{\mu\nu} + (Q^2 - \Pi_L) C^{\mu\nu} + \Pi_d D^{\mu\nu}] D_{\text{ret}}^A \quad (\text{B1})$$

where

$$D_{\text{ret}}^A = \frac{1}{(Q^2 - \Pi_L)(Q^2 - \Pi_c) - \frac{Q^2 g^2}{q_0^2} \Pi_d^2} \quad (\text{B2})$$

and

$$D_{\text{ret}}^B = \frac{1}{Q^2 - \Pi_e}. \quad (\text{B3})$$

The tensors $P_T^{\mu\nu}$ and $P_L^{\mu\nu}$ are the same as in thermal equilibrium while $C^{\mu\nu}$ and $D^{\mu\nu}$ are new tensors that depend on the anisotropy vector \mathbf{n} . The self-energy components

Π_e , Π_L , Π_T and Π_d are given in [47] which contains further details.

As $\Pi_d = \mathcal{O}(\xi)$ we can approximate

$$D_{\text{ret}}^A \approx \frac{1}{(Q^2 - \Pi_L)(Q^2 - \Pi_c)} \quad (\text{B4})$$

up to order $\mathcal{O}(\xi)$. We furthermore ignore $\mathcal{O}(\xi)$ corrections in the numerator as they do not describe anisotropic corrections to screening which are the non-equilibrium corrections we focus on. Then

$$\begin{aligned} D_{\text{ret}}^{\mu\nu}(Q) &\approx (P_T^{\mu\nu} - C^{\mu\nu}) D_{\text{ret}}^B \\ &\quad + [(Q^2 - \Pi_c) P_L^{\mu\nu} + (Q^2 - \Pi_L) C^{\mu\nu}] D_{\text{ret}}^A \\ &= \frac{P_T^{\mu\nu} - C^{\mu\nu}}{Q^2 - \Pi_e} + \frac{P_L^{\mu\nu}}{Q^2 - \Pi_L} + \frac{C^{\mu\nu}}{Q^2 - \Pi_c} \end{aligned} \quad (\text{B5})$$

The terms with the tensor $C^{\mu\nu}$ go like

$$C^{\mu\nu} \left[\frac{-1}{Q^2 - \Pi_e} + \frac{1}{Q^2 - \Pi_c} \right] = C^{\mu\nu} \frac{\Pi_c - \Pi_e}{(Q^2 - \Pi_e)(Q^2 - \Pi_c)} \quad (\text{B6})$$

which can be ignored as $\Pi_c - \Pi_e = \mathcal{O}(\xi)$ in the numerator. We are thus left with

$$D_{\text{ret}}^{\mu\nu}(Q) \approx \frac{P_T^{\mu\nu}}{Q^2 - \Pi_e} + \frac{P_L^{\mu\nu}}{Q^2 - \Pi_L}. \quad (\text{B7})$$

at small anisotropy where we only include anisotropic corrections in the denominators. The tensors P_L and P_T are the same as in equilibrium while Π_e and Π_L have anisotropic corrections. (We call $\Pi_e = \Pi_T$ in the main text of the paper.)

Appendix C: Details of numerical method

In this Appendix we discuss how to solve Eqs. (35) and (36) numerically. Unlike the isotropic equation, Eq. (31), the anisotropic equation has a non-vanishing source term on the right hand side for all values of b . One thus needs a different numerical solution method than that developed in [48, 53, 54] for the equilibrium case. We note that the differential equation for the function $f_1^{(3)}$ is

$$\begin{aligned} \mathcal{K} [f_1^{(3)}(\mathbf{b})] + \frac{ik}{2p(p+k)} \frac{8}{b^2} f_1^{(3)}(\mathbf{b}) + \mathcal{C}_0(b) f_1^{(3)}(\mathbf{b}) \\ = -\frac{1}{2} \mathcal{C}_1^{(b)}(b) f_0 \end{aligned} \quad (\text{C1})$$

but we will not discuss this function further as it is not needed to evaluate A_z and A_y in Eqs. (38) and (39)

For concreteness, we focus on solving Eq. (35). Defining a scaled function

$$G = \frac{\pi}{2} \frac{k}{p(p+k)m_{\infty}^2} \frac{f_1^{(1z)}(b)}{b}, \quad (\text{C2})$$

as well as scaled collision kernels $\bar{\mathcal{C}}(t) = \frac{2p(p+k)}{k} \frac{1}{m_\infty^2} \mathcal{C}(b)$ and variable $t = m_\infty b$, this equation becomes

$$\begin{aligned} -i \left[\frac{d^2 G}{dt^2} + \frac{3}{t} \frac{dG}{dt} - G \right] + \bar{\mathcal{C}}_0(t) G \\ = - \left[\bar{\mathcal{C}}_1^{(a)}(t) + \frac{1}{2} \bar{\mathcal{C}}_1^{(b)}(t) \right] \bar{f}_0(t) \end{aligned} \quad (\text{C3})$$

where $\bar{f}_0(t) = \frac{\pi}{2} \frac{k}{p(p+k)m_\infty^2} \mathbf{b} \cdot \mathbf{f}_0/b^2$. As shown in [48], we can write $\bar{f}_0(t) = K_1(t)/t + \bar{f}_0^{\text{rest}}(t)$ where $\bar{f}_0^{\text{rest}}(t)$ is function that is finite in the limit $t \rightarrow 0$ and which we know numerically using the methods of [48, 53].

We need to solve Eq. (C3), imposing the boundary conditions that $G(t) \rightarrow 0$ as $t \rightarrow \infty$, as well as that $G(t)$ is finite as $t \rightarrow 0$. These boundary conditions are difficult to satisfy simultaneously for a numerical solution. Instead we find a numerical solutions $g(t)$ of Eq. (C3) with $g(t \rightarrow \infty) = 0$ and a solution of the homogeneous equation without the source term that also satisfies $g_0(t \rightarrow \infty) = 0$. In general, both $g(t)$ and $g_0(t)$ blow up as $t \rightarrow 0$. However, we know that the solution we are seeking can be written as

$$G(t) = g(t) + A g_0(t) \quad (\text{C4})$$

where A is chosen so that $G(0)$ is finite.

We can find an explicit expression of A by using analytic solutions of Eq. (C3) for $t \ll 1$. In that limit the right hand side is

$$\begin{aligned} \left[\bar{\mathcal{C}}_1^{(a)}(t) + \frac{1}{2} \bar{\mathcal{C}}_1^{(b)}(t) \right] \bar{f}_0(t) \\ \approx \left[\bar{\mathcal{C}}_1^{(a)}(t) + \frac{1}{2} \bar{\mathcal{C}}_1^{(b)}(t) \right] K_1(t)/t \approx a + b \log t \end{aligned} \quad (\text{C5})$$

where a and b are constants that depend on the momenta k and p as well as the masses m_D^2 and m_∞^2 . The differential equation becomes

$$-i \left[\frac{d^2 g}{dt^2} + \frac{3}{t} \frac{dg}{dt} - g \right] + \bar{\mathcal{C}}_0(t) g = a + b \log t \quad (\text{C6})$$

which has general solution

$$g(t) = w(t) + \alpha_1 w_1(t) + \alpha_2 w_2(t) \quad (\text{C7})$$

where

$$w(t) = -ia - ib(\log t + \frac{2}{t^2}) \quad (\text{C8})$$

is an exact particular solution and $w_2(t) = 2J_1(it)/(it)$ and $w_1(t) = \frac{\pi}{2} Y_1(-it)/(-it) - \frac{1}{4}(2\gamma_E - 2 \log 2 + i\pi) w_2(t)$ are solutions of the homogeneous equation such that $w_1(t) = 1/t^2 + \frac{1}{2} \log t + \mathcal{O}(1)$ and $w_2(t) = \mathcal{O}(1)$ for small t . Similarly, the homogeneous equation can be written as

$$g_0(t) = \beta_1 w_1(t) + \beta_2 w_2(t). \quad (\text{C9})$$

The coefficients $\alpha_1, \alpha_2, \beta_1$ and β_2 can be found from Eqs. (C7) and (C9) by equating the numerical solutions $g(t)$ and $g_0(t)$ and their derivatives with the analytic functions at some small value $t_{\min} \ll 1$.

The small t behaviour of Eqs. (C7) and (C9) shows that

$$A = \frac{2ib - \alpha_1}{\beta_1} \quad (\text{C10})$$

which makes

$$G(0) = -ia - \frac{1}{2} ib + \alpha_2 + \frac{(2ib - \alpha_1)\beta_2}{\beta_1} \quad (\text{C11})$$

finite. This is the expression that we need in order to evaluate Eq. (38). All quantities are known for numerical solutions $g(t)$ and $g_0(t)$.

Eq. (C11) suffers from numerical cancellation errors in the terms $\alpha_2 - \alpha_1 \beta_2 / \beta_1$. It is thus better to rewrite these terms using Eqs. (C7) and (C9) which shows that

$$\alpha_2 - \frac{\alpha_1 \beta_2}{\beta_1} = \frac{g' g_0 - g g'_0 + g'_0 w - g_0 w'}{g_0 w'_2 - g'_0 w_2}. \quad (\text{C12})$$

where all quantities are evaluated at $t_{\min} \ll 1$. The culprit behind cancellation errors is the term $g' g_0 - g g'_0$. It can be evaluated more precisely by noting that

$$\mathcal{G}_W(t) = g'(t) g_0(t) - g(t) g'_0(t). \quad (\text{C13})$$

solves the equation

$$\frac{d(t^3 \mathcal{G}_W)}{dt} = -it^3 \left[\bar{\mathcal{C}}_1^{(a)}(t) + \frac{1}{2} \bar{\mathcal{C}}_1^{(b)}(t) \right] \bar{f}_0(t) g_0 \quad (\text{C14})$$

which can be integrated to give $\mathcal{G}_W(t_{\min})$ and thus a reliable value of $G(0)$.

[1] See, for example, G. Aarts *et al.*, Phase Transitions in Particle Physics – Results and Perspectives from Lattice Quantum Chromo-Dynamics (2023) arXiv:2301.04382 [hep-lat], and references therein.

[2] See, for example, Y. Aoki, G. Endrodi, Z. Fodor, S. D.

Katz, and K. K. Szabo, The Order of the quantum chromodynamics transition predicted by the standard model of particle physics, *Nature* **443**, 675 (2006), arXiv:hep-lat/0611014, and references therein.

[3] W. Busza, K. Rajagopal, and W. van der Schee,

- Heavy Ion Collisions: The Big Picture, and the Big Questions, *Ann. Rev. Nucl. Part. Sci.* **68**, 339 (2018), arXiv:1802.04801 [hep-ph].
- [4] M. Strickland, Small system studies: A theory overview, *Nucl. Phys. A* **982**, 92 (2019), arXiv:1807.07191 [nucl-th].
- [5] R. Snellings (STAR, ALICE), Anisotropic flow from RHIC to the LHC, *Eur. Phys. J. C* **49**, 87 (2007), arXiv:nucl-ex/0610010.
- [6] M. Connors, C. Nattrass, R. Reed, and S. Salur, Jet measurements in heavy ion physics, *Rev. Mod. Phys.* **90**, 025005 (2018), arXiv:1705.01974 [nucl-ex].
- [7] G. David, Direct real photons in relativistic heavy ion collisions, *Rept. Prog. Phys.* **83**, 046301 (2020), arXiv:1907.08893 [nucl-ex].
- [8] P. Salabura, Dilepton production in heavy ion collisions, *Acta Phys. Polon. B* **39**, 307 (2008).
- [9] M. R. Heffernan, C. Gale, S. Jeon, and J.-F. Paquet, Bayesian quantification of strongly-interacting matter with color glass condensate initial conditions, (2023), arXiv:2302.09478 [nucl-th].
- [10] D. Everett *et al.* (JETSCAPE), Phenomenological constraints on the transport properties of QCD matter with data-driven model averaging, *Phys. Rev. Lett.* **126**, 242301 (2021), arXiv:2010.03928 [hep-ph].
- [11] D. Everett *et al.* (JETSCAPE), Multisystem Bayesian constraints on the transport coefficients of QCD matter, *Phys. Rev. C* **103**, 054904 (2021), arXiv:2011.01430 [hep-ph].
- [12] J. E. Bernhard, J. S. Moreland, and S. A. Bass, Bayesian estimation of the specific shear and bulk viscosity of quark-gluon plasma, *Nature Phys.* **15**, 1113 (2019).
- [13] J. S. Moreland, J. E. Bernhard, and S. A. Bass, Alternative ansatz to wounded nucleon and binary collision scaling in high-energy nuclear collisions, *Phys. Rev. C* **92**, 011901 (2015), arXiv:1412.4708 [nucl-th].
- [14] B. Schenke, P. Tribedy, and R. Venugopalan, Fluctuating Glasma initial conditions and flow in heavy ion collisions, *Phys. Rev. Lett.* **108**, 252301 (2012), arXiv:1202.6646 [nucl-th].
- [15] B. Schenke, S. Jeon, and C. Gale, (3+1)D hydrodynamic simulation of relativistic heavy-ion collisions, *Phys. Rev. C* **82**, 014903 (2010), arXiv:1004.1408 [hep-ph].
- [16] B. Schenke, S. Jeon, and C. Gale, Elliptic and triangular flow in event-by-event (3+1)D viscous hydrodynamics, *Phys. Rev. Lett.* **106**, 042301 (2011), arXiv:1009.3244 [hep-ph].
- [17] J.-F. Paquet, C. Shen, G. S. Denicol, M. Luzum, B. Schenke, S. Jeon, and C. Gale, Production of photons in relativistic heavy-ion collisions, *Phys. Rev. C* **93**, 044906 (2016), arXiv:1509.06738 [hep-ph].
- [18] C. Shen, Z. Qiu, H. Song, J. Bernhard, S. Bass, and U. Heinz, The iEBE-VISHNU code package for relativistic heavy-ion collisions, *Comput. Phys. Commun.* **199**, 61 (2016), arXiv:1409.8164 [nucl-th].
- [19] M. Bleicher *et al.*, Relativistic hadron hadron collisions in the ultrarelativistic quantum molecular dynamics model, *J. Phys. G* **25**, 1859 (1999), arXiv:hep-ph/9909407.
- [20] J. Weil, V. Steinberg, J. Staudenmaier, L. G. Pang, D. Oliinychenko, J. Mohs, M. Kretz, T. Kehrenberg, A. Goldschmidt, B. Bäuchle, J. Auvinen, M. Attems, and H. Petersen, Particle production and equilibrium properties within a new hadron transport approach for heavy-ion collisions, *Phys. Rev. C* **94**, 054905 (2016).
- [21] S. Cao *et al.* (JETSCAPE), Determining the jet transport coefficient q from inclusive hadron suppression measurements using Bayesian parameter estimation, *Phys. Rev. C* **104**, 024905 (2021), arXiv:2102.11337 [nucl-th].
- [22] C. Gale, Photon Production in Hot and Dense Strongly Interacting Matter, *Landolt-Bornstein* **23**, 445 (2010), arXiv:0904.2184 [hep-ph].
- [23] S. Hauksson, S. Jeon, and C. Gale, Photon emission from quark-gluon plasma out of equilibrium, *Phys. Rev. C* **97**, 014901 (2018), arXiv:1709.03598 [nucl-th].
- [24] S. Hauksson, S. Jeon, and C. Gale, Probes of the quark-gluon plasma and plasma instabilities, *Phys. Rev. C* **103**, 064904 (2021), arXiv:2012.03640 [hep-ph].
- [25] G. Baym and T. Hatsuda, Polarization of Direct Photons from Gluon Anisotropy in Ultrarelativistic Heavy Ion Collisions, *PTEP* **2015**, 031D01 (2015), arXiv:1405.1376 [nucl-th].
- [26] B. Schenke and M. Strickland, Photon production from an anisotropic quark-gluon plasma, *Phys. Rev. D* **76**, 025023 (2007), arXiv:hep-ph/0611332.
- [27] L. Bhattacharya, R. Ryblewski, and M. Strickland, Photon production from a nonequilibrium quark-gluon plasma, *Phys. Rev. D* **93**, 065005 (2016), arXiv:1507.06605 [hep-ph].
- [28] P. B. Arnold, G. D. Moore, and L. G. Yaffe, Photon emission from ultrarelativistic plasmas, *JHEP* **11**, 057, arXiv:hep-ph/0109064.
- [29] P. B. Arnold, G. D. Moore, and L. G. Yaffe, Photon emission from quark gluon plasma: Complete leading order results, *JHEP* **12**, 009, arXiv:hep-ph/0111107.
- [30] P. B. Arnold, G. D. Moore, and L. G. Yaffe, Photon and gluon emission in relativistic plasmas, *JHEP* **06**, 030, arXiv:hep-ph/0204343.
- [31] J. Ghiglieri, J. Hong, A. Kurkela, E. Lu, G. D. Moore, and D. Teaney, Next-to-leading order thermal photon production in a weakly coupled quark-gluon plasma, *JHEP* **05**, 010, arXiv:1302.5970 [hep-ph].
- [32] R. Baier, H. Nakkagawa, A. Niegawa, and K. Redlich, Production rate of hard thermal photons and screening of quark mass singularity, *Z. Phys. C* **53**, 433 (1992).
- [33] J. I. Kapusta, P. Lichard, and D. Seibert, High-energy photons from quark - gluon plasma versus hot hadronic gas, *Phys. Rev. D* **44**, 2774 (1991), [Erratum: *Phys.Rev.D* 47, 4171 (1993)].
- [34] H.-U. Yee, Flows and polarization of early photons with magnetic field at strong coupling, *Phys. Rev. D* **88**, 026001 (2013), arXiv:1303.3571 [nucl-th].
- [35] S.-Y. Wu and D.-L. Yang, Holographic Photon Production with Magnetic Field in Anisotropic Plasmas, *JHEP* **08**, 032, arXiv:1305.5509 [hep-th].
- [36] D. Ávila, T. Monroy, F. Nettel, and L. Patiño, Emission of linearly polarized photons in a strongly coupled magnetized plasma from the gauge/gravity correspondence, *Phys. Lett. B* **817**, 136287 (2021), arXiv:2101.08802 [hep-th].
- [37] L. Dong and S. Lin, Dilepton helical production in a vortical quark-gluon plasma, *Eur. Phys. J. A* **58**, 176 (2022), arXiv:2112.07153 [hep-ph].
- [38] K. A. Mamo and H.-U. Yee, Spin polarized photons and dileptons from axially charged plasma, *Phys. Rev. D* **88**, 114029 (2013), arXiv:1307.8099 [nucl-th].
- [39] A. Ipp, A. Di Piazza, J. Evers, and C. H. Keitel, Photon polarization as a probe for quark-gluon plasma dynamics, *Phys. Lett. B* **666**, 315 (2008), arXiv:0710.5700 [hep-ph].

- [40] G. Baym, T. Hatsuda, and M. Strickland, Virtual photon polarization in ultrarelativistic heavy-ion collisions, *Phys. Rev. C* **95**, 044907 (2017), arXiv:1702.05906 [nucl-th].
- [41] E. Shuryak, Monitoring parton equilibration in heavy ion collisions via dilepton polarization, (2012), arXiv:1203.1012 [nucl-th].
- [42] E. Speranza, A. Jaiswal, and B. Friman, Virtual photon polarization and dilepton anisotropy in relativistic nucleus–nucleus collisions, *Phys. Lett. B* **782**, 395 (2018), arXiv:1802.02479 [hep-ph].
- [43] P. Aurenche, F. Gelis, R. Kobes, and H. Zaraket, Bremsstrahlung and photon production in thermal QCD, *Phys. Rev. D* **58**, 085003 (1998), arXiv:hep-ph/9804224.
- [44] R. K. Ellis, W. J. Stirling, and B. R. Webber, *QCD and collider physics*, Vol. 8 (Cambridge University Press, 2011).
- [45] P. Romatschke and M. Strickland, Collective modes of an anisotropic quark gluon plasma, *Phys. Rev. D* **68**, 036004 (2003), arXiv:hep-ph/0304092.
- [46] M. Martinez and M. Strickland, Dissipative Dynamics of Highly Anisotropic Systems, *Nucl. Phys. A* **848**, 183 (2010), arXiv:1007.0889 [nucl-th].
- [47] S. Hauksson, S. Jeon, and C. Gale, Momentum broadening of energetic partons in an anisotropic plasma, *Phys. Rev. C* **105**, 014914 (2022), arXiv:2109.04575 [hep-ph].
- [48] P. Aurenche, F. Gelis, and H. Zaraket, A Simple sum rule for the thermal gluon spectral function and applications, *JHEP* **05**, 043, arXiv:hep-ph/0204146.
- [49] S. Caron-Huot, O(g) plasma effects in jet quenching, *Phys. Rev. D* **79**, 065039 (2009), arXiv:0811.1603 [hep-ph].
- [50] M. Panero, K. Rummukainen, and A. Schäfer, Lattice Study of the Jet Quenching Parameter, *Phys. Rev. Lett.* **112**, 162001 (2014), arXiv:1307.5850 [hep-ph].
- [51] G. D. Moore, S. Schlichting, N. Schlusser, and I. Soudi, Non-perturbative determination of collisional broadening and medium induced radiation in QCD plasmas, *JHEP* **10**, 059, arXiv:2105.01679 [hep-ph].
- [52] S. Mrowczynski, B. Schenke, and M. Strickland, Color instabilities in the quark–gluon plasma, *Phys. Rept.* **682**, 1 (2017), arXiv:1603.08946 [hep-ph].
- [53] P. Aurenche, F. Gelis, G. D. Moore, and H. Zaraket, Landau-Pomeranchuk-Migdal resummation for dilepton production, *JHEP* **12**, 006, arXiv:hep-ph/0211036.
- [54] S. Jeon and G. D. Moore, Energy loss of leading partons in a thermal QCD medium, *Phys. Rev. C* **71**, 034901 (2005), arXiv:hep-ph/0309332.
- [55] M. E. Peskin and D. V. Schroeder, *An Introduction to quantum field theory* (Addison-Wesley, Reading, USA, 1995).